Available online at www.sciencedirect.com
SCIENCE DIRECT®
Catalysis Today 93–95 (2004) 55–63
CATALYSIS TODAY
www.elsevier.com/locate/cattod

Development of bimodal cobalt catalysts for Fischer–Tropsch synthesis

Yi Zhang, Misao Shinoda, Noritatsu Tsubaki*

Department of Applied Chemistry, School of Engineering, Toyama University, Gofuku 3190, Toyama 930-8555, Japan

Available online 2 July 2004

Abstract

A new and simple method for preparing multi-functional nano-sized silica-silica or zirconia-silica bimodal pore catalyst support was developed by direct introduction of silica or zirconia sols into silica gel. The pores of the obtained bimodal pore supports distributed distinctly as two kinds of main pores. On the other hand, the increased BET surface area and decreased pore volume, compared to those of original silica gel, indicated that the obtained bimodal pore supports formed according to the designed route, and it is found that the zirconia-silica bimodal support improved catalyst activity significantly via not only spatial effect, the intrinsic property of the bimodal structure, but also chemically promotional effect of zirconia, when this kind of support was applied in the liquid-phase Fischer–Tropsch synthesis (FTS) as a cobalt-loading catalyst.

Keywords: Bimodal pore support; Fischer–Tropsch synthesis (FTS); Pore size control; Cobalt catalyst; Zirconia

1. Introduction

Metallic cobalt is an excellent catalyst for CO hydrogenation, yielding higher hydrocarbons in FTS [1]. The activity of supported cobalt catalyst in the FTS should be proportional to the area of the exposed metallic cobalt atoms [2,3]. The high dispersion of the cobalt metal is usually done by deposition of a cobalt salt on high surface area supports, such as silica and alumina, and subsequent reduction. The support with large surface area, however, usually contains small pore size, which results in poor intra-pellet diffusion efficiency of reactants and products, especially in multi-phase reactor. Slow transportation of reactants to and products from catalytic sites often controls the rate of primary and secondary reactions even on small catalyst pellet [4]. Meanwhile, the pore size of catalyst also affects product selectivities, due to the spatial effect of support. In contrast, the bimodal pore structure support, which contains large pores and small pores at the same time, contribute to higher dispersion of supported cobalt crystalline by the small pores, which enlarges the surface area of support. Furthermore, it is able to diminish the diffusion resistance by its large pores. A support with a distinct bimodal pore structure has excellent advantages in solid catalysis reaction because the large pores provide pathways for rapid molecular transportation and small pores serve a large area of active surface, contributing to high diffusion efficiency and high dispersion of supported metal simultaneously, as theoretically expressed by Levenspiel [5].

Until now, several preparation methods were reported to form bimodal pore catalyst support. But these methods used very corrosive reagents such as aqua regia, and the size of large pores of the obtained bimodal structure was as high as several hundred nanometers that the effect of bimodal structure was not obvious [6,7]. Furthermore, the reported methods are only effective for one specific oxide support, such as Al_2O_3 or SiO_2. A general method to prepare bimodal structure, especially containing hetero-atom structure, is expected.

To find a simple, clean, and general preparation method to form tailor-made bimodal pore structure, we propose here a new method to introduce silica or zirconia sols into large-pore silica gel directly to form the bimodal pore supports. As an application of this kind of bimodal pore support, it was used for liquid-phase FTS reactions after cobalt was supported. Meanwhile, as a promoter of Co/SiO_2 FTS catalyst, zirconia should promote the catalytic activity as well [8].

* Corresponding author. Tel.: +81 76 445 6846; fax: +81 76 445 6846.
E-mail address: tsubaki@eng.toyama-u.ac.jp (N. Tsubaki).

0920-5861/$ – see front matter © 2004 Elsevier B.V. All rights reserved.
doi:10.1016/j.cattod.2004.05.013

2. Experimental

2.1. Catalyst preparation

The bimodal support was prepared by incipient-wetness impregnation of a commercially available silica gel (Cariact Q-50, Fuji Silysia Co., specific surface area: 70 $m^2\,g^{-1}$; pore volume: 1.2 $ml\,g^{-1}$; pellet size: 74–590 μm; and mean pore diameter: 50 nm), with zironia sol (Seramic G 401, Nibban Institute Co., paticle size: 1.7–2.4 nm, content: 21 wt.%, alcohol solution) or silica sol (Snowtex XS, Nissan Chemicals Co.; particle size: 5 nm; content: 20 wt.%; aqueous solution). After the impregnation, the support was calcined in air at 673 or 873 K for 2 h directly without drying, for zirconia or silica bimodal, respectively.

Cobalt-supported catalyst with 10 wt.% metal loading was prepared by incipient-wetness impregnation of different supports, including the bimodal ones, with cobalt nitrate aqueous solution. The catalyst precursors were dried in air at 393 K for 12 h, then calcined in air from room temperature to 673 K with a ramping rate of 2 $K\,min^{-1}$ and kept at 673 K for 2 h. After calcination, the catalysts were activated in flowing hydrogen at 673 K for 10 h, and at last, passivated by 1% oxygen in nitrogen at room temperature for 1 h.

2.2. Reaction apparatus

FTS reaction was carried out in a semi-batch autoclave, slurry-phase reactor with the inner volume of 80 ml. The passivated catalyst (1.0 g, under 149 μm) and 20 ml liquid medium (*n*-hexadecane) were loaded in the reactor. During the reaction, effluent gas released from the reactor was analyzed by on-line gas chromatography. CO and CO_2 were analyzed by using an active charcoal column equipped with a thermal conductivity detector (TCD). The hydrocarbons were also analyzed using FID for C_1-C_5 (Porapak Q, on-line) and for C_6–C_{20} (SE-30, uniport), respectively. Argon was employed as an internal standard with concentration of 3% in the feed gas. The reaction conditions were P (total) = 1.0 MPa, CO/H_2 = 1/2, W/F (CO + H_2 + Ar) = 10 $g\,h\,mol^{-1}$, T = 513 K.

2.3. Catalyst characterization

Pore size distribution, BET surface area and pore volume were determined by a measuring instrument for surface area and pore size of porous materials (Shimadzu ASAP 2000) where nitrogen was used as absorbent. Supported cobalt crystalline size of the passivated catalysts was detected by TEM (TOPCON EM-002B; acc. volt: 200 kV; point resolution: 0.18 nm; line resolution: 0.14 nm) and XRD (Rigaku, RINT2000). The supported cobalt crystalline average size was calculated by $\sum n_i {d_i}^3 / \sum n_i {d_i}^2$ for TEM data and by $L = K\lambda/\Delta(2\theta)\cos\theta_0$ for XRD data, where L is the crystallite size, K is a constant (K = 0.9–1.1), λ is the wavelength of X-ray (Cu Kα = 0.154 nm), and $\Delta(2\theta)$ is the width of the peak at half height. In this study, the 2θ of 44° for two kinds of bimodal catalysts and 42° for Q-3 catalyst were used to calculate the supported cobalt crystalline size.

Thermal gravimetric analysis (TGA) was conducted using a Shimadzu DTG-60 instrument. The samples before calcination were placed in the furnace and heated in air from room temperature to the desired temperature, 873 K, at a heating rate of 10 $K\,min^{-1}$ and then held at final temperature for 2 h.

Temperature-programmed reduction (TPR) experiments were carried out in a quartz-made microreactor using 0.2 g calcined catalysts. The gas stream, 5% H_2 diluted by nitrogen as reducing gas, was fed via a mass flow controller. After the reactor, the effluent gas was led via a 3 Å molecular sieve trap to remove the produced water, before entering TCD.

In situ FTIR spectra of various catalysts were collected by a Nicolet Nexus 470 FT-IR spectrometer with a MCT detector. In situ absorbance spectra were obtained by collecting 32 scans at 2 cm^{-1} resolution. The passivated catalyst powder 14 mg was contained in an infrared cell. The samples were reduced in the cell at 673 K for 1 h. After purging the infrared cell by He, the adsorbent (CO) was introduced into cell at room temperature and atmospheric pressure with 10 $ml\,min^{-1}$ for 10 min. And then, the CO was purged by He before the FTIR spectra of the CO adsorption were measured at the room temperature under He flow.

3. Results and discussion

3.1. Design and characterization of bimodal pore supports

The pore size distributions of silica gel Q-50 and bimodal pore supports were shown in Fig. 1. It is clearly proved that the obtained silica bimodal support contained 6 and 45 nm pores meantime, unlike uniformly distributed silica gel Q-50. In calcination step, it is considered the small particles from silica sols formed 6 nm small pores through dehydration occurred between the surface OH-groups of silica sol particles, inside the large pores of silica gel. The large pore of silica gel Q-50 slightly decreased from original 50–45 nm in bimodal structure.

The BET surface area significantly increased from 70 to 132 $m^2\,g^{-1}$ for silica bimodal due to the newly-formed small pores, as compared in Table 1. As the loaded particles of silica sols formed silica porous structure inside the large pores of Q-50, the pore volume of obtained bimodal support decreased. The BET surface area increased and pore volume decreased with the increased loading of silica, as shown in Table 1 also.

Concerning the pore distributions, the obtained bimodal pore support distinctly exhibited two kinds of pores according to bimodal pore structure. The increased BET surface area and decreased pore volume indicated that the particles

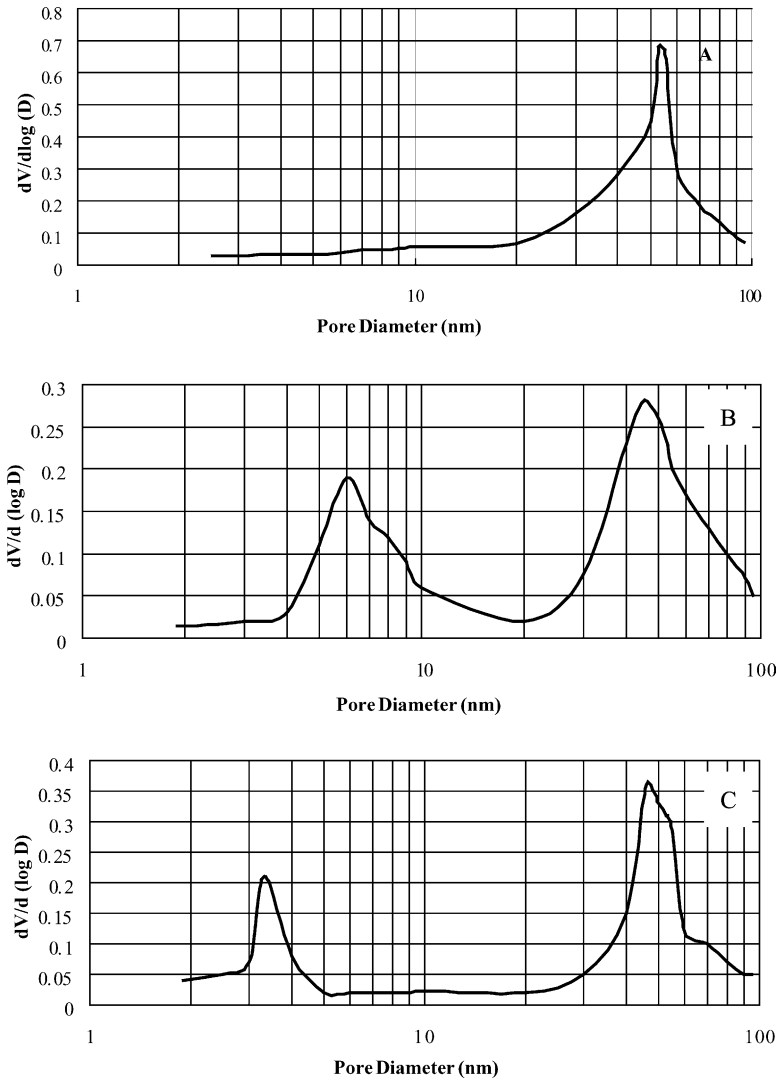

Fig. 1. The pore size distributions of Q-50 and the bimodal pore supports (A) Q-50. (B) Silica bimodal pore support. (C) Zirconia bimodal pore support. (B) The weight ratio of silica from silica sol to Q-50 silica was 11.2%. (C) The weight ratio of zirconia from zirconia sol to Q-50 silica was 16.8%.

of silica sols entered the original large pores indeed, and deposited on the inner surface of Q-50 to form the small pores, as illustrated in Fig. 2. The pore size formation of bimodal pore support depended on newly-formed silica porous structure inside the large pores of Q-50. If the sol-derived silica particles blocked the pore structure of Q-50 and did not form the new small pores inside the large pores, the BET surface area would decrease remarkably. Based on these findings, it is able to conclude that the obtained bimodal support formed according to the designed route, as shown in Fig. 2.

It was reported that the particles of silica sol aggregated easily when vapor coexisted in calcination step, because the silanol on the surface of silica particles was easy to produce, contributing to movement of the particles of silica sol [9]. Based on this, the samples of silica bimodal supports

Table 1
Characteristics of various supports

Support	SiO_2 or ZrO_2 loading (wt.%)	BET ($m^2\,g^{-1}$)	Pore diameter (nm)	Pore volume ($ml\,g^{-1}$)
Q-50	0.0	70	50.0	1.20
Q-3	0.0	546	3.0	0.30
Silica bimodal A1	5.6	88	6.0-45	0.65
Silica bimodal A2	11.2	106	6.0-45	0.46
Silica bimodal A3	22.5	132	6.0-45	0.40
Zirconia bimodal	16.8	201	3.2-45	0.41

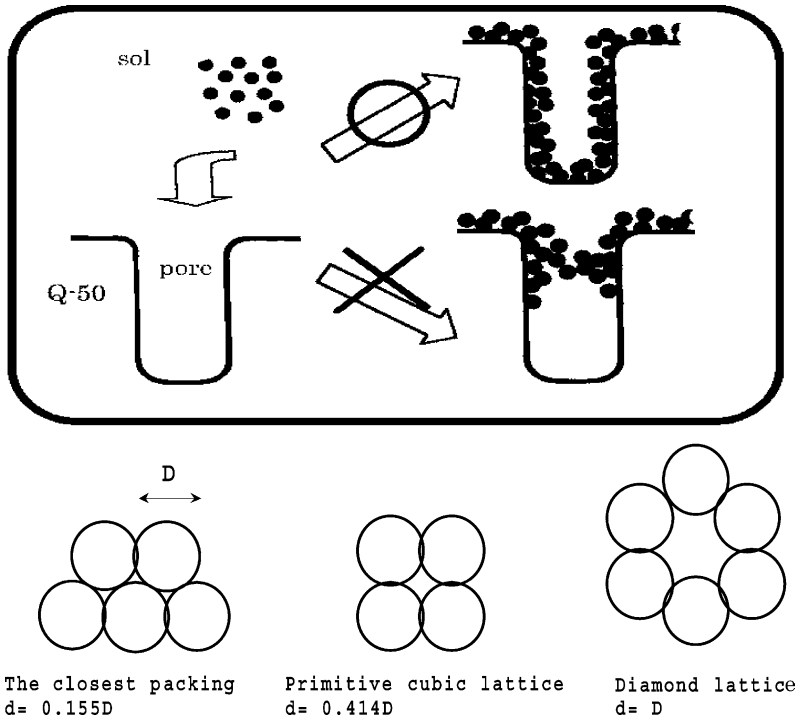

Fig. 2. Formation scheme of the bimodal pore support.

were calcined at 873 K for 2 h directly without drying after impregnation to improve the aggregation of silical sols particles with the coexisting vapor and formation of new small pores. Concerning the TGA of the calcination step of the silica bimodal support sample, as shown in Fig. 3, an endothermic weight loss was found at 355 K, due to the vaporization of water. After removal of solvent water, the dehydration of silanol occurred on the surface of the silica particles, resulting in aggregation of the silica particles to form the 6 nm small pores inside the large pores of silica Q-50.

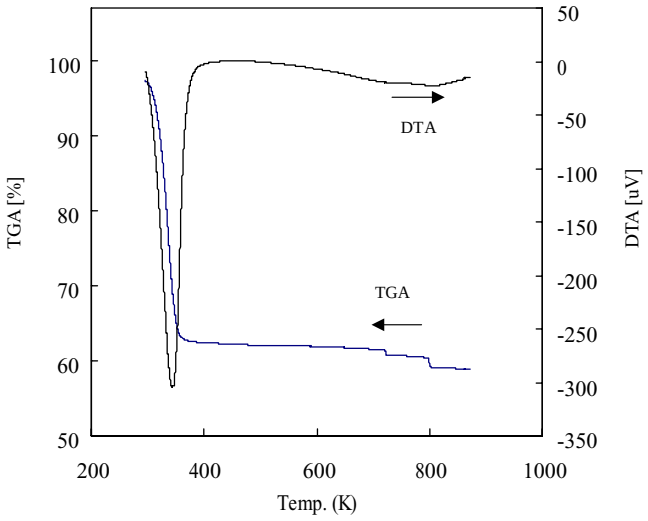

Fig. 3. The TG and DTA profiles of silica bimodal pore support sample. The weight ratio of silica from silica sols to Q-50 silica was 11.2%.

The endothermic weight loss between 727 and 800 K was attributed to this dehydration of silanol groups of the silica sols particles. There was no weight loss when the samples were held at 873 K for 2 h.

For a mass of agglomerate of spherical particles, specific surface area (S) is given by following equations:

$$S = \frac{3}{\rho r} \quad (1)$$

where r and ρ are the radius and density of the particles, respectively. Based on this, the specific surface area of silica bimodal pore support can be determined by the particle size of silica sols, namely one can choose a kind of sol with favorite particle size to form a desired pore size distribution for bimodal pore support. Furthermore, if the diameter of a primary particle in sol is D, the pore size, produced by this kind of primary particles, is determined by diameter D and the agglutination of primary particles [10]. It will be $0.155D$, $0.414D$ and D, when the primary particles aggregate as closest packing, primitive cubic lattice and diamond lattice, respectively, as shown in Fig. 2. In this study, the primary particle size of silica sol was 5 nm, and it formed new small pores inside the large pores of silica gel Q-50 as 6 nm. The more important point was that for obtained silica bimodal pore supports, the newly-formed small pore size was 6 nm, irrespective of the increased silica loading, as exhibited in Table 1. These findings indicated that the primary particles of silica sol aggregated as diamond lattice mainly, inside the large pores of silica Q-50 in the calcination step. If the primary particles mainly aggregated as closest packing or primitive cubic lattice, the size of newly-formed small

pores would be smaller than the diameter of primary particle. If the primary particles at first formed the secondary particles mainly, and the latter formed new small pore, the size of newly-formed small pores would vary with the changed silica loading. Furthermore, it is confirmed that the specific surface area and pore structure of porous silica support were thermally stable until 1200 K. Therefore the specific surface area and pore structure of obtained bimodal supports were not influenced by the calcination temperature, which was 873 K in this study. Based on these findings, it was considered that the silica bimodal pore support with desired large pores and small pores was able to be formed by choosing a silica gel with suitable large pores and a silica sol with favorite particle size. It is our target to form just two kinds of pore sizes, not continuously distributed pore size. Small pores are not directly from the original 50 nm large pore. The small pores are formed by self-assembly of nanoparticles from sol, according to diamond lattice mode, inside the original large pores, a kind of confined space. As small pore formed inside the inner surface of large pores, large pore size decreased from its original 50–45 nm, as illustrated in Fig. 2.

Meanwhile, a lot of oxides, such as zirconia, were used as promoter to synthesize highly active silica-base FTS catalyst [11]. By introducing different sols other than SiO_2 sols into silica pellets, the multi-functional bimodal pore support can be formed, where besides spatial effect of bimodal pore structure, new chemical phenomenon or effect might appear with the hetero-atom formation between different oxides. In this study, the zirconia-silica bimodal pore support was formed by using zirconia sols and silica pellets. For the obtained zirconia bimodal support, the specific surface area increased from 70 $m^2\,g^{-1}$ of silica gel Q-50 to 201 $m^2\,g^{-1}$. And pore volume decreased from 1.2 $ml\,g^{-1}$ of Q-50 to 0.41 $ml\,g^{-1}$ of zirconia bimodal pore support, as shown in Table 1. The pores of the obtained zirconia bimodal pore support distinctly distributed as two kind of pore size, as 3.2 and 45 nm, according to bimodal structure, as exhibited in Fig. 1.

3.2. The reaction performance of different bimodal pore catalysts

To investigate the promotional role of the bimodal supports, it was applied to liquid-phase Fischer–Tropsch synthesis reaction. Liquid-phase Fischer–Tropsch synthesis reaction has advantages in temperature control, wax extraction and catalyst lifetime extension, compared to the common gas-phase reaction [12]. But the main drawback of the liquid-phase FTS reaction was the slow diffusion rate of the syngas as well as the formed hydrocarbons. To release the overall reaction from possible diffusion-controlled regime and obtain maximum hydrocarbon yield, silica bimodal support with 11.2 wt.% silica loading and zirconia bimodal support with 16.8 wt.% zirconia loading were used to prepare the cobalt-supported catalysts, which were tested in liquid-phase FTS reaction.

The reaction performance of the catalysts prepared from the bimodal support or Cariact Q-50, Q-3 was compared in Table 2. Cariact Q-3 was an analogy to Q-50 but with average pore size of 3nm. Their properties were compared in Table 1. Catalyst prepared from Q-3 support had the largest surface area but the smallest pore diameter. It exhibited low catalytic activity and the highest methane selectivity. For the catalyst prepared from Q-50 support, which had the lowest surface area and the largest pore size, the CO conversion, CH_4 and CO_2 selectivity were the lowest. For the catalyst prepared from silica bimodal support, the CO conversion was higher than that of catalyst derived from Q-50 and Q-3, and meanwhile selectivities of CH_4 and CO_2 were as low as to those of the catalyst prepared from Q-50. For the zriconia bimodal catalyst, the CO conversion was significantly increased from that of silica bimodal catalyst as the highest in this study, and the selectivities of CH_4 and CO_2 were almost the same as those of silica bimodal catalyst.

It has been already pointed out that the propagation of the carbon–carbon chain occurred more easily on the catalyst with lower specific surface area where metallic particle

Table 2
Characteristics of various catalysts

Catalysts	BET of support ($m^2\,g^{-1}$)	CO Conv. (%)	Sel.[a] (%)		Co crystal size (nm)		Co Disp.[b]	Reduction degree[c]/TPR (%)	TOF[d] ($10^{-2}\,s^{-1}$)	C_5^+ (%)	α
			CH_4	CO_2	XRD	TEM					
Q-50	70	17	7.1	3.2	35.0	37.0	2.55	98.6	3.51	83	0.86
Silica bimodal	106	33	10.1	2.7	20.2	22.6	3.63	86.2	4.39	83	0.86
Zirconia bimodal	201	86	11.0	3.2	23.6	21.6	4.70	88.1	13.41	85	0.87
Q-3	546	26	22.0	20.5	4.5	1.4	38.21	62.3	0.94	81	0.84

Reaction conditions: 513 K; 1.0 MPa; $W/F = 10\,g\,h\,mol^{-1}$; $H_2/CO = 2$; cobalt loading: 10 wt.%. Turnover frequency (TOF) is the rate of per surface cobalt atom; $TOF = n_{co}X(CO)/^n$Co surface (s^{-1}). X (CO): CO conversion; n: molecular or atom number; α: chain growth probability.

[a] Calculated by: $Sel._{methane} = 100\% \times M\ CH_4/(\text{converted CO} - M\ CO_2)$ $Sel._{carbondioxide} = 100\% \times M\ CO_2/\text{converted CO}$; M: amount of formed CH_4 or CO_2 (mol).

[b] Calculated by H_2 chemisorption at 373 K.

[c] Calculated from 373 to 1073 K.

[d] Used the reduction degree from TPR.

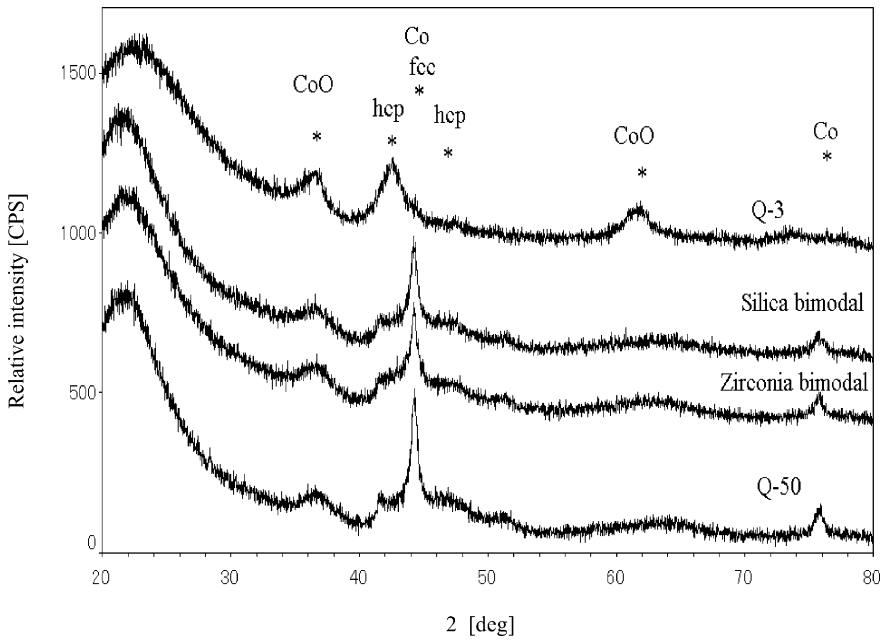

Fig. 4. The XRD patterns of various catalysts. SiO_2 bimodal: the weight ratio of silica from silica sol to Q-50 silica was 11.2%. ZiO_2 bimodal: the weight ratio of zirconia from zirconia sol to Q-50 silica was 16.8%.

size was larger [13,14], which naturally decreased methane formation. When the pore size was larger, the transportation of the primary product was more effective and relevantly methane formation rate from secondary hydrocracking of olefins was lower. Also lower BET surface area of large-pore support determined larger metallic size and suppressed methane formation. On the other hand, the activities and selectivities of the FTS catalysts are markedly depending on their pore structure. The catalyst having a small pore size tended to produce lighter hydrocarbons. However, the product distribution of large-pore catalyst was wider and the proportion of the heavy hydrocarbon was high [15,16]. Based on these reasons, the methane selectivity was the lowest for the catalyst prepared from Q-50. Due to the larger pore existing in the catalyst prepared from bimodal support, the CH_4 selectivity was also low. The hydrocarbon products of all catalysts were agreed well with the Anderson-Schulz-Flory products distribution. The chain growth probability and C_5^+ selectivity did not change significantly. The chain growth probability was 0.86, 0.86, 0.87and 0.84 of the catalysts derived from Q-50, silica bimodal, zirconia bimodal and Q-3, respectively, as shown in Table 2. Q-3 with the smallest pore exhibited the lowest chain growth probability, proving that large pore was favorite for chain propagation.

3.3. Catalyst structure

On the other hand, FTS rates on cobalt catalyst can be improved by increasing the dispersion of supported cobalt crystalline. Generally, the metal dispersion is increased with the increased surface area and the decreased pore size of support. The supported cobalt crystalline average size was calculated by the data of TEM, as 37, 22.6, 21.6 and 1.4 nm for Q-50 catalyst, silica bimodal pore catalyst, zirconia bimodal pore catalyst, and Q-3 catalyst, respectively, as presented in Table 2. For Q-3 derived catalyst, its small pore and slow diffusion efficiency determined high methane selectivity. But its CO conversion was not the highest, regardless of its highest metal dispersion in this study. The supported cobalt crystalline size was detected also by XRD. The XRD spectra of various catalysts were shown in Fig. 4. This clearly displays that the catalysts prepared from bimodal supports had smaller particle sizes than that of the catalyst prepared from silica gel Q-50. In Table 2, the metal particle size calculated by XRD data is generally in accordance with that from TEM. The supported cobalt dispersion was determined by H_2 chemisorption at 373 K also, as shown in Table 2. It was clear that the dispersion of two kinds of bimodal pore catalysts was higher than that of Q-50 catalyst and lower than that of Q-3 catalysts. Based on these findings, it was proved that the dispersion of the supported cobalt was improved by the bimodal pore structure.

The average pore size increased very slightly for various Co/SiO_2 catalysts, compared to the corresponding bimodal pore support. Since the supported cobalt crystalline blocked some smaller pores of support, but the bimodal pore catalysts still kept bimodal structure with two kinds of pore size of 8 and 47 nm for silica bimodal catalyst, as well as 5 and 47 nm for zirconia bimodal catalyst, as shown in Fig. 5. Bimodal catalyst, having higher metal dispersion due to its larger BET surface area, and accelerated diffusion rate derived from the

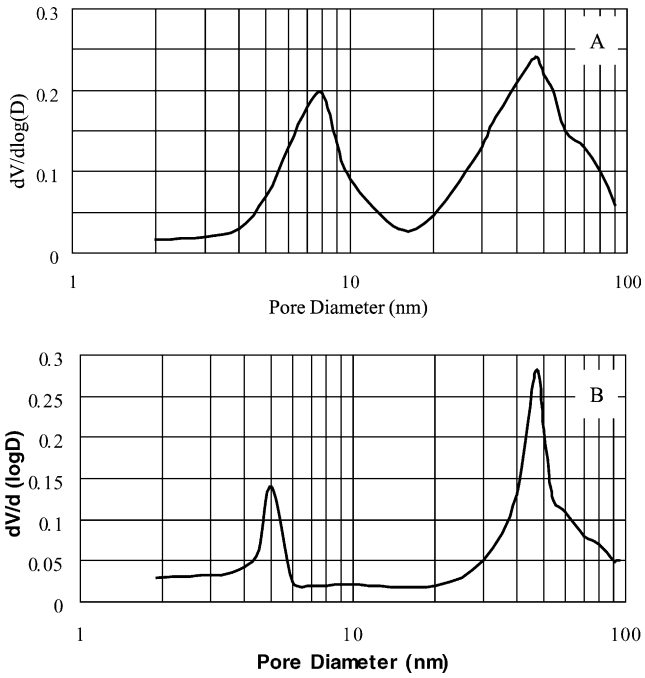

Fig. 5. The pore size distribution of bimodal pore catalysts with Co loading of 10 wt.%. (A) SiO_2 bimodal: the weight ratio of silica from silica sol to Q-50 silica was 11.2%. (B) ZiO_2 bimodal: the weight ratio of zirconia from zirconia sol to Q-50 silica was 16.8%.

bimodal structure, exhibited the highest CO conversion and low methane selectivity.

3.4. Promotional effect from ZrO_2

It has been claimed that in low-pressure FTS, addition of zirconia to the Co/Al_2O_3 catalyst support led to markedly increased activity and C_5^+ selectivity but this phenomenon was not due to the increased cobalt dispersion and a change in the reducibility [17]. Withers et al. found an increase in activity for FTS with increasing Zr/Co ratio for Co on ZrO_2/SiO_2 support using a slurry-phase reactor [11]. Ali et al reported that cobalt on ZrO_2/SiO_2 did not exhibit such a high dispersion effect and had the same reduction degrees as the un-promoted catalyst. But zirconia addition to Co/SiO_2 significantly increased the specific reaction rate of FTS [18].

In this study, the reduction property of various catalysts was detected by TPR. In TPR spectra of various catalysts, as shown in Fig. 6, two peaks existed for the Q-50 catalyst, which located at 612 and 673 K. The two peaks have been identified as conversion Co^{3+} to Co^{2+} followed by the conversion of Co^{2+} to Co, and the broad region that was located above 800 K indicated the existence of several species reduced at approximately the same temperature [19]. For the Q-3 catalyst, the first peak located at 610 K and the second peak was rising from 700 K, while the H_2 consumption continuously increased until 1073 K, indicating that some Co could not be reduced at lower temperatures. For silica bimodal catalyst, there was only one wide peak from 500 to 820 K. On the other hand, the TPR spectra of zirconia bimodal catalyst exhibited three peaks, which located at 610, 673 and 752 K. Especially, the first peak was more intensive than the second and the third peak. Comparing the reduction degrees of various catalysts, which were calculated by TPR data from 323 to 1073 K, the Q-50 catalyst showed the best reducibility as 98.6% due to its largest supported cobalt particle which had lighter interaction with silica support. For Q-3 catalyst, due to its smallest supported cobalt particles, which had the strong interaction with silica support, the reducibility was the lowest as 62.3%. Both of two kinds of bimodal catalysts showed almost the same reducibility, as

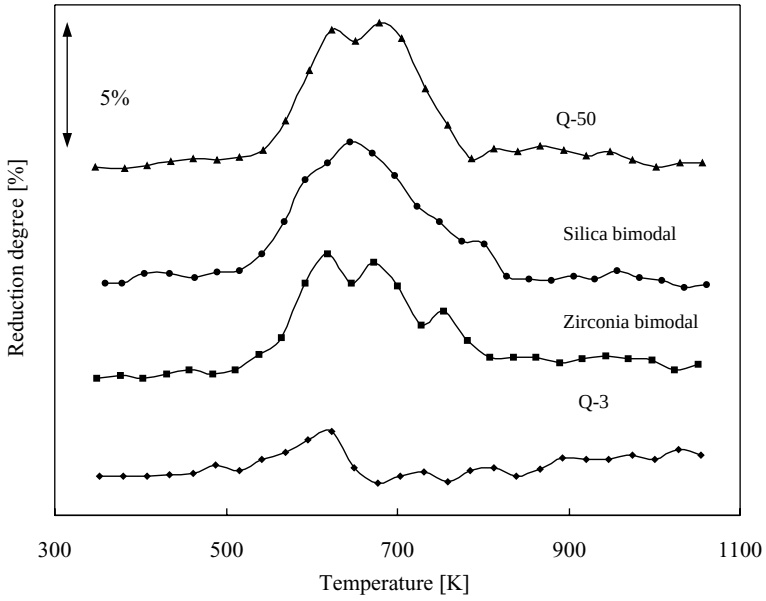

Fig. 6. TPR spectra of different catalysts with Co loading of 10 wt.%. SiO_2 bimodal: the weight ratio of silica from silica sol to Q-50 silica was 11.2%. ZiO_2 bimodal: the weight ratio of zirconia from zirconia sol to Q-50 silica was 16.8%.

86.2% for silica bimodal pore catalyst and 88.1% for zirconia bimodal pore catalysts.

In this study, it is considered that zirconia, which formed the new small pores of bimodal support, influenced the reduction performance due to some chemical effects, but did not improve the reduction degree of supported cobalt crystalline. Furthermore, on bimodal pore catalyst, the dispersion of supported cobalt crystalline was improved due to enlarged BET surface area by the newly-formed zirconia porous structure inside original large pore, not attributed to chemical promotional effect of zirconia. A number of authors proposed that on zirconia modified cobalt silica catalysts, CO dissociation was facilitated, leading to an increase in reaction rate [20,21]. The TOF of different catalysts was calculated in this study also. As shown in Table 2, the TOF of zirconia bimodal catalyst was significantly higher than that of silica bimodal catalyst, even though their reduction degree and crystalline size of supported cobalt were almost the same. Hence, the results suggest that the activity of Co sites might be increased due to the presence of ZrO_2 in zirconia bimodal catalyst. ZrO_2 might form an active interface with Co, which was responsible, to some extent, for the enhancement in Co activity.

3.5. In situ FT-IR measurement

The FT-IR spectra of the adsorbed CO for the reduced catalysts are compared in Fig. 7. Many studies report one band in the 2000–2050 cm^{-1} range after CO adsorption. This band has been attributed to linearly bonded molecules with surface cobalt atoms [22,23]. In our investigation, this adsorbed species manifested itself by a band at 2035, 2037, 2039 and 2047 cm^{-1} for Q-50, silica bimodal, zirconia bimodal and Q-3 catalyst, respectively. In general, the blue shift of this band indicated that the C–O band became strong if the CO adsorbed onto small cobalt particles. The band of CO adsorbed on Co metal in linear mode shifted from 2035 cm^{-1} for Q-50 catalyst to 2047 cm^{-1} for Q-3 catalyst here, as the metallic particle size of silica bimodal, zirconia bimodal and Q-3 catalyst was smaller than that of Q-50 catalysts, as shown in Table 2.

The 2057 cm^{-1} shoulder peak can be assigned to the surface carbonyl species, which readily happened to corner sites on the cobalt metal, and the bands of 1939 and 1937 cm^{-1} are attributed to the bridge-type CO adsorbed on cobalt metal particles [24,25]. For the two kinds bimodal pore catalysts, the peak of bridged adsorbed CO was stronger than that of Q-50 catalyst. For zirconia bimodal catalyst, the peak of bridged adsorbed CO was the strongest. For the Q-3 catalyst, the species of bridged adsorbed CO was not detected. As pointed out, the bridged adsorbed CO was much more active than linearly adsorbed CO [26]. The high activity of bimodal catalysts can be attributed to the increase in bridge-type adsorbed CO, which was easily dissociated to carbon and oxygen, especially zirconia bimodal catalyst.

3.6. Extension of this preparation method

From described above, it is clear that building up micropores using zirconia particles inside silica large pores realized two functionality, chemical promotion and spatial promotion, at the same time to enhance the activity for liquid-phase FTS reaction. One was the bimodal pore structure with both large and small pores in the supports, which improved the diffusion rate of syngas and products, and the dispersion of active metal particles, respectively. The other was the presence of zirconia in the bimodal supports, which itself acted as a catalytic promoter for FTS reaction. These results indicate that a new, simple and general method for preparing bimodal support is developed by manipulation of zirconia

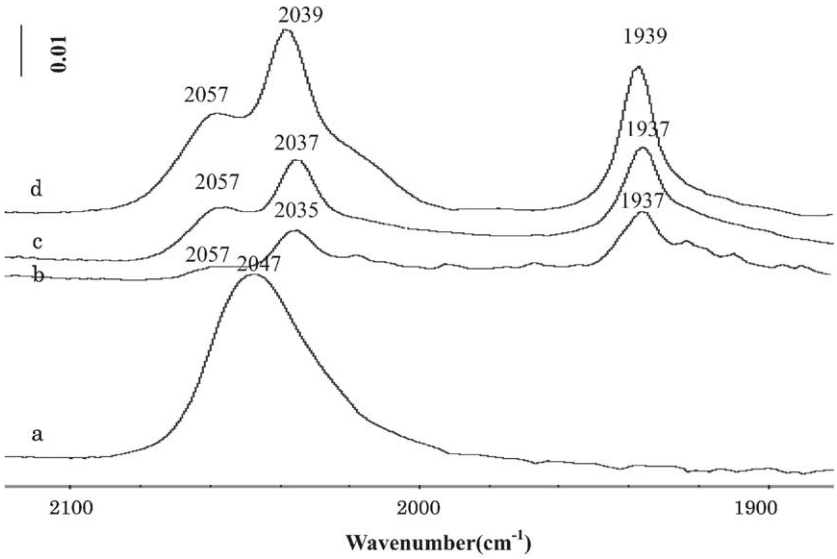

Fig. 7. In situ FT-IR CO spectra of various catalysts at room temperature. (a) Q-3; (b) Q-50; (c) SiO_2 bimodal; (d) ZrO_2 bimodal.

nano-particles from its sol inside the pores of silica gel. By this method, the multi-functional bimodal pore support with both large and micropores of the desired size can be easily prepared and the pore sizes of the bimodal pore structure are successfully controlled.

Furthermore, building small pores using A oxide like a "brick" via its sol inside large pores of B oxide can easily extended to prepare a lot of kinds of bimodal supports if varying A and B [27]. Besides spatial effect of bimodal pore structure, new chemical phenomenon or effect might appear with the hetero-atom formation between A and B. This method can be expanded to prepare various bimodal structure catalyst supports with different chemical compositions as it is possible to change the combination of large-pore gel and sol. For instance, Al_2O_3-SiO_2 (large pore: Al_2O_3, small pore: SiO_2), SiO_2-SiO_2 or SiO_2-Al_2O_3 (large pore: SiO_2, small pore: Al_2O_3) bimodal structure is also possible.

4. Conclusions

The method of introducing oxide sols into the large pore silica pellet, to form tailor-made bimodal catalyst support, was developed. The distinctly distributed two kinds of pores, the increased BET surface area and the decreased pore volume of the obtained bimodal support proved that the particles from the sol indeed entered the uniformly distributed intrinsic large pores of silica pellet to ensure bimodal structure.

The Co/SiO_2 catalysts derived from silica bimodal supports were tested in slurry-phase FTS. It showed higher activity and favorable selectivities, due to its improved dispersion of supported cobalt crystalline by bimodal structure, as proved by XRD and TEM, and fastened diffusion efficiency inside catalyst pellet with bimodal structure. Furthermore, besides the spatial effect from bimodal structure as shown in silica-silica bimodal catalyst, significantly enhanced activity was realized using ZrO_2-SiO_2 bimodal support, as ZrO_2 inside the large pores of SiO_2 not only formed small pores but also intrinsically promoted FT synthesis.

References

[1] M.A. Vannice, J. Catal. 50 (1977) 228.
[2] E. Igleasia, S.L. Soled, R.A. Fiato, J. Catal. 137 (1992) 212.
[3] E. Iglesia, Appl. Catal. A 161 (1997) 59.
[4] E. Iglesia, S.C. Reyes, R.J. Madon, J. Catal. 129 (1991) 238.
[5] O. Levenspiel, Chemical Reaction Engineering, 2nd ed., Wiley, New York, 1972, p. 496.
[6] R. Takahashi, S. Sato, T. Sodesawa, M. Yabuki, J. Catal. 200 (2001) 197.
[7] T. Inui, M. Funabiki, M. Suehiro, T. Sezume, J. Chem. Soc. Faraday I 75 (1979) 787.
[8] A. Hoek, A.H. Joustra, J.K. Minderhould, M.F. Post, UK Patent Application GB 2 125062 A, 1983.
[9] R. Iler, Colloid Chemistry of Silica and Silicates, Cornell University Press, 1955.
[10] M.F.L. Jhonson, J. Mooi, J. Catal. 10 (1968) 353.
[11] H.P. Withers Jr., K.F. Eliezer, J.W. Mitchell, Ind. Eng. Chem. Res. 29 (1990) 1807.
[12] L. Fan, K. Yokota, K. Fujimoto, Topics Catal. 22 (1995) 67.
[13] H.H. Nijs, P.A. Jacobs, J. Catal. 65 (1980) 328.
[14] K. Fujimoto, T. Nobusawa, T. Fukushima, H. Tominaga, Bull. Chem. Soc. Jpn. 58 (1985) 3164.
[15] L. Fan, K. Yokota, K. Fujimoto, AIChE J. 38 (1992) 1639.
[16] S. Sun, N. Tsubaki, K. Fujimoto, J. Chem. Eng. Jpn. 33 (2000) 232.
[17] F. Rohr, O.A. Lindvag, A. Holmen, Z.A. Blekkan, Catal. Today 58 (2000) 247.
[18] S. Ali, B. Chen Jr., J.G. Goodwin, J. Catal. 157 (1995) 35.
[19] M.P. Rosynek, C.A. Polansky, Appl. Catal. 73 (1991) 97.
[20] M. Ichikawa, T. Fukushima, J. Phys. Chem. 89 (1985) 1564.
[21] A.L. Borer, C. Bronnimann, R. Prins, J. Catal. 145 (1994) 516.
[22] M.J. Heal, E.C. Leisegang, R.G. Torington, J. Catal. 51 (1978) 314.
[23] K. Mohana Rao, D. Scarano, G. Spoto, A. Zecchina, Surf. Sci. 204 (1988) 319.
[24] R.C. Reuel, C.H. Bartholomew, J. Catal. 85 (1984) 63.
[25] N. Tsubaki, S. Sun, K. Fujimoto, J. Catal. 199 (2001) 236.
[26] E. Iglesia, S.L. Soled, R.A. Fiato, G.H. Via, J. Catal. 143 (1993) 345.
[27] Y. Zhang, Y. Yoneyama, N. Tsubaki, Chem. Comm. (2002) 1216.